

## Shear rate behaviour within *in vitro* thrombotic geometries: height and surface curvature dependence.

C. J. Butler<sup>1,2</sup>, I. Pinar<sup>1,3</sup>, K. Ryan<sup>1</sup>, J. Carberry<sup>1,3</sup> and G. J. Sheard<sup>1,3</sup>

<sup>1</sup>Department of Mechanical and Aerospace Engineering  
 Building 31, Monash University, Victoria 3800, Australia

<sup>2</sup>IBM Research – Australia  
 Level 5, 204 Lygon Street, Carlton, Victoria 3053, Australia

<sup>3</sup>Division of Biological Engineering, Faculty of Engineering  
 Clayton Campus, Monash University Victoria 3800, Australia

### Abstract

The flow of blood past thrombi, situated within an *in vitro* geometry, is computed via the solution to the three-dimensional (3D) Navier–Stokes equations. The thrombotic geometry is derived from microscopy measurements of thrombotic geometries within *in vitro* experiments which the *in silico* experiment reflects. The flow within the numerical domain is solved using the OpenFOAM package to provide an solution of the steady state and incompressible Navier–Stokes equations. Previous work (Butler et al, 2012) explored the shear rate variations that occur in a simplified thrombotic geometry. Here additional flow complexity is introduced through the complexity of the thrombus geometry. Localised fluctuations of the thrombus surface are shown to generate significant variations in the shear-rate the thrombus surface experiences. Convex and exposed surfaces are shown to have the highest shear rates. In addition to the concavity the height above the microchannel floor is shown to correlate strongly with increased shear rate.

### Introduction

Thrombosis, the development of blood clots within the vasculature, presents a significant clinical risk of myocardial infarction, cerebral and pulmonary embolism, and other diseases. Studies have long shown that there is an interaction between vascular diseases and the dynamics of blood flow (for a review see [7]). However, the quantification of flow effects on thrombus growth is more recent. In general a thrombus is an aggregate of blood cells and proteins bound to a blood vessel wall. The structure of the thrombus under arterial conditions is dominated by platelets. As a result the growth of a thrombus, under arterial conditions, is dependent on the aggregation, adhesion and activation of platelets [9]. An important question may be posed; after initial formation of a thrombus what interactions mediate platelet adhesion and activation after isolation of the injury site?

In addition to the biochemical processes that occur, early studies [1] showed shear force dependent platelet functionality at pathological shear rates ( $\gamma \geq 10000$ ). Note that within these experiments  $\gamma \geq 10000$  for a substantial period of time Further research revealed that shear rate correlates with the adhesive potential of platelets [11]. However, recent research, particularly that of Nesbitt et al. [9], has shown a causal relationship between shear-force and the initial adhesion and recruitment of a platelet to a thrombus. Critically the physical recruitment occurs in the absence of chemical agonists previously thought to be required for recruitment [6]. It was also theorized that spatial ‘micro-gradients’ of shear are required for shear mediated platelet aggregation [9, 13].

The current state of the art method for studying platelet adhe-

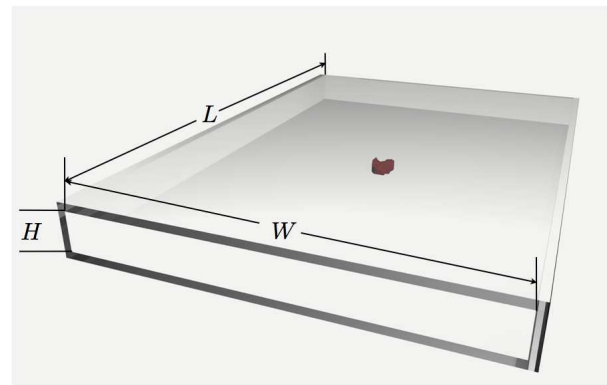


Figure 1: Illustration of the numerical domain. Flow runs through from bottom left to top-right of the page. Red mass at the center of the channel represents the thrombus.

sion *in vitro* can be found summarized in [8]. Importantly we note that there is no consideration of the non-linear effects of the Navier–Stokes equations on shear rate. Shear rate is approximated globally by Poiseuille flow:  $\gamma_{P_w} = \frac{6U}{H}$ , where  $U$  is the mean flow velocity,  $H$  is the height of the channel and  $\gamma_{P_w}$  shear rate at the wall of a channel presuming Poiseuille flow conditions. Our previous work [2, 3, 4] explored a thrombus analogue with a simplified geometry that has shown that changing the thrombus size and  $\gamma_{P_w}$  significantly changes both the amplitude of shear rate and the topology of shear rate on the surface of the thrombus. In this paper we seek to tightly couple our *in silico* experiments with *in vitro* experiments. Flow will be computed around thrombotic geometries derived thrombotic geometries from the experiments previously presented within [13].

### Methodology

The thrombotic geometry considered by this study was derived from the experiments conducted with [13]. The first part of this section will discuss the *in vitro* model and the acquisition of the thrombotic geometry. The later parts will discuss the numerical techniques for the fluid flow and required post-processing techniques.

The *in vitro* fluid flow is based on that of a high aspect ratio microchannel. Here the channel as aspect ratio (AR) where:

$$AR = \frac{W}{H} \quad (1)$$

where  $W$  is the width of the channel and  $H$  the height. The length  $L$  of these channels is such that  $L : H$  is 500 : 1 for this

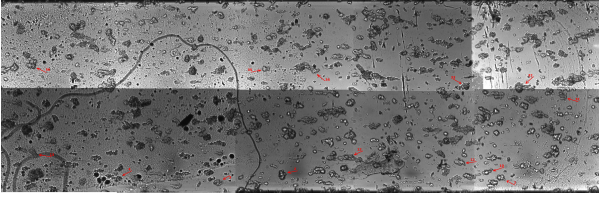


Figure 2: Bright field microscopy images of a partial *in vitro* microchannel. The vertical extent of the tiled images is approximately wall-to-wall across the width of the channel, with flow being left to right across the page. Identifiable thrombi are marked by red arrows. Image courtesy of Dr. Elham Tolouei, from the experiments reported in [13].

study. This geometry is shown diagrammatically within figure 1. These geometries the standard methodology for considering shear dependent platelet adhesion and are used widely (for example see [6, 9, 11] and others). The channel employed in this case has  $H = 200 \mu\text{m}$  and here we are examining the cases where the flow rate is set such that  $\gamma_{P_w} = 1800$  presuming there is no influence of the growing thrombi on the channel wall. Within this channel a thrombus is introduced as a protuberance from the lower wall into the channel, this is shown within figure 1 as the red mass within the channel. Within this study eight individual thrombi are separately introduced into their own numerical channel. They are introduced such that the centroid of the thrombus (of the cross section at the channel wall) is located at the centre of the channel with respect to length and width. Details of how the thrombus geometry is obtained is discussed within the ‘*in vitro* methodology’ section.

The Reynolds number for the system is defined as for channel flow:

$$\text{Re} = \frac{UH}{\nu}, \quad (2)$$

where  $\nu$  is the kinematic viscosity. Given the high wall shear rate of the experiment ( $\gamma_{P_w} = 1800$ ), and the flow rate, and therefore the flow, a Newtonian model for blood flow is considered to be acceptable [10]. Matching the *in vitro* channel allows a linear relationship between  $\gamma_{P_w}$  and  $\text{Re}$  to be derived as:  $\text{Re} = 4.34 \times 10^6 - 3\gamma_{P_w}$ , allowing  $\nu$  to be found as required. Using this setup eight thrombus geometries are considered for this study.

Previously we have shown that  $\gamma_{P_w}$  is insufficient to characterise shear rate in the vicinity of thrombotic geometries [2]. Therefore local shear rate follows the previous model,

$$\gamma = \sqrt{2} \sqrt{S : S}, \quad (3)$$

where,

$$S = \nabla \mathbf{u} + (\nabla \mathbf{u})^T. \quad (4)$$

Shear rate is scaled relative to  $\gamma_{P_w}$ ,

$$\chi = \frac{\gamma}{\gamma_{P_w}}. \quad (5)$$

#### *in vitro* method to mesh generation.

Extended details of the biological setup are beyond the scope of this paper and are discussed fully within [13] and the references contained within. Here we briefly describe the details relevant to this study. The walls of the microchannel are coated with a thrombogenic material to allow thrombi to develop on the interior surface. A syringe pump is used to generate a steady state flow rate of whole blood until the thrombi within the microchannel reach a steady state size. At this point a fixative agent is used

to fix the thrombi to the surface within the channel, allowing the profiles of the thrombi to be digitised at a later time.

Figure 2 is an example of a small sample of the thrombotic geometry that is generated *in vitro*. Here a number of thrombi are identified on the surface of the channel. These thrombi are individually digitised with a bright-field microscopy technique presented within [13]. The brightfield microscopy technique allows thrombi to be scanned on an individual basis. A surface approximation of the thrombus is generated according to the method presented in [13]. A base numerical mesh is generated as a grid of cubic elements where the size is defined by the number across the channel height  $N$  where the edge length  $\Delta z = \frac{H}{N}$ . Cubic mesh and the thrombus surface approximation are merged using the process described within [5] to create a numerical approximation of the channel including the thrombotic geometry.

#### Numerical technique

This study considers blood as an incompressible, Newtonian fluid. The flow is considered to be unsteady within the previously described channel. This approximation yields the Navier–Stokes equations to be solved as

$$\frac{\partial \mathbf{u}}{\partial t} + \mathbf{u} \cdot \nabla \mathbf{u} = -\nabla P + \nu \nabla^2 \mathbf{u}, \quad (6)$$

$$\nabla \cdot \mathbf{u} = 0, \quad (7)$$

where  $\nu$  is the kinematic viscosity,  $\mathbf{u}$  is the velocity vector field and  $P$  is the kinematic pressure field. Here the OpenFOAM® numerical solver is employed to solve the incompressible Navier–Stokes equations to a steady state using the SIMPLE algorithm [12]. The algorithm operates over a arbitrary polyhedral finite volume mesh maintaining second order accuracy in space with the advection operator employing the QUICK scheme. Both a domain size study and a grid resolution study were performed for the computational mesh described previously. A mesh was chosen where  $\frac{L}{H} = 12$  and  $\frac{H}{\Delta z} = 20$  as the point where the error was less than 0.1% with respect to the largest domain size and highest resolution cases, respectively (data not shown).

#### Boundary conditions

There are three separate types of boundary conditions: The input to the channel, the output from the channel and the solid boundaries. The solid boundaries include the side, upper and lowers walls in addition to the thrombus surface. The solid boundaries have a Dirichlet boundary condition for velocity  $\mathbf{u} = 0$ , and a Neumann boundary condition for pressure. The outlet has a Neumann boundary condition for velocity and a Dirichlet pressure condition  $P = 0$ . The inlet boundary has a Neumann pressure condition in addition to the prescription of the analytic solution to laminar flow in a rectangular channel (see [2]).

#### Results and Discussion

All of the thrombi are solved to a steady state with residuals of  $\mathbf{u}$  and  $\mathbf{p}$  are less than  $10^{-10}$ . Figure 3 examines two thrombi that have been selected to be representative of the set of thrombi considered. Each sub-figure (3a and 3b) considers a particular thrombus, where the left hand and centre frames display  $\chi$ . Examining the centre frame for each thrombus, where fluid flows from left to right, as the fluid approaches the thrombus on the channel wall, the shear rate decreases from  $\chi = 1$  towards  $\chi = 0$  at the interface between the lower wall and the thrombus surface. The low shear region surrounding the thrombus and on the lower wall reflects the paradigm of Nesbitt et al. [9] where

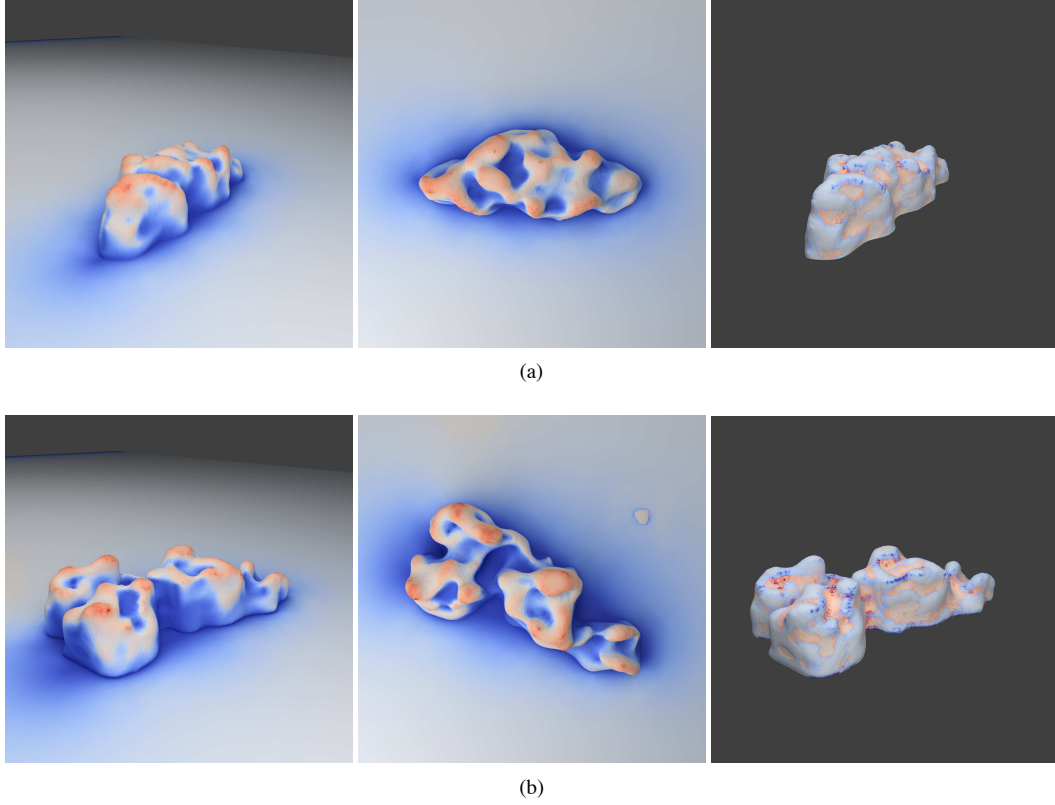


Figure 3: Contours of  $\chi$  and  $\kappa$  on the thrombus surface and the surrounding microchannel floor. The left two frames are of  $\chi$ . Colouring spectrum: blue, white and red, represents  $\chi = 0$ ,  $\chi = 1$  and  $\chi = 8$  respectively. Flow is from bottom left to top right and left to right, in the left and middle frames, respectively. The right hand frame is colored by  $\kappa$  with the same view as the left hand frame.

low shear regions at the rear of the thrombus are the platelet aggregation zones. Here we see that the surface topology of the thrombus is complex with many pockets and protuberances across the surface. The high protuberances directly exposed to the flow appear to have higher  $\chi$  than the concave pockets which appear to have  $\chi \ll 1$ .

The right hand frame of figures 3a and 3b displays the surface curvature of the thrombus surface. Here it is seen that the regions of high shear correlate with convex surfaces. It is noted that while this is visually true it is not a linear, regions of extreme curvature do not necessarily correlate with extreme  $\chi$ . The nature of the three dimensional surface creates a difficult in understanding the correlation between surface curvature, shear rate, and position on the surface. Figure 4 is an attempt to reduce the data such that this is possible. A set of bivariate bins, with respect to both curvature,  $\kappa$ , and height on the thrombus (as a fraction of channel height),  $h$ , are established. Every mesh vertex on the surface of the thrombus is allocated to a bin based on  $\kappa$  and  $h$ . If one surface mesh vertices exist within a bin the coloring is based on the the mean of  $\chi$  for the vertices in the bin. Note that negative and positive  $\kappa$  represent convex and concave regions, respectively. Here the strong correlation between height on the thrombus surface and  $\chi$  is clear. Large  $\chi$  is focused on a region where  $h$  is large  $h$  and  $\kappa < 0$ . It is noted that for  $h \approx \max(h)$  that  $\chi$  is high for both positive and negative  $\kappa$ . We note that for both thrombi there is a region at a lower  $h$  and  $\kappa < 0$  where large  $\chi$  is observed.

The results of figures 3 and 4 paint a picture: Points protruding into the flow have high  $\chi$ . The thrombus is acting as a bluff body and consequently the surfaces on the thrombus which are ‘exposed’ to the flow have high  $\chi$ . Figure 5 summarised the ef-

fect of  $\kappa$  across a number of surfaces. Here a clear trend is seen: regions of high shear are highly convex. Here a gross estimation of where high  $\chi$  regions occur may be made from  $\kappa$  and  $h$ . The link between  $\kappa$  and  $\chi$  can be elucidated by considering the vorticity generated as the flow follows around a curved surface. Consider the flow near the surface to act as solid body rotation where:

$$\mathbf{u}_\theta = \frac{1}{2}\omega\mathbf{r}, \quad (8)$$

However, given a fixed  $\mathbf{u}_\theta$  (flow velocity tangential to the surface) as  $r$  decreases (or  $\kappa$ ) increases, vorticity on the surface increases. As  $\chi$  and  $\omega$  are analogous in two dimensional flows it can be approximated as

$$\chi \propto |\kappa| \quad (9)$$

for convex surfaces. The reverse will hold true for concave surfaces: where the surface curvature will act to negate the vorticity generated by the flow at the surface. The increased geometric complexity generates significant and highly localised variations in  $\chi$  increasing the complexity of thrombotic flows. Yet despite this clear trends are seen. In addition to the local complexity the overall behaviour of ‘low–high–low’ behavior  $\chi$  observed previously has been maintained [2, 9, 13].

## Conclusions

This numerical investigation has explored the dynamics of shear rate, surrounding a thrombotic geometry within an *in vitro* environment. Global behaviour has been maintained with previous *in vitro* and *in silico* studies, yet, highly complex  $\chi$  behaviour is observed on the thrombus surface. The complex behaviour has been shown to correlate with the surface curvature and height - potentially allowing a simplified model of  $\chi$  to be formed.

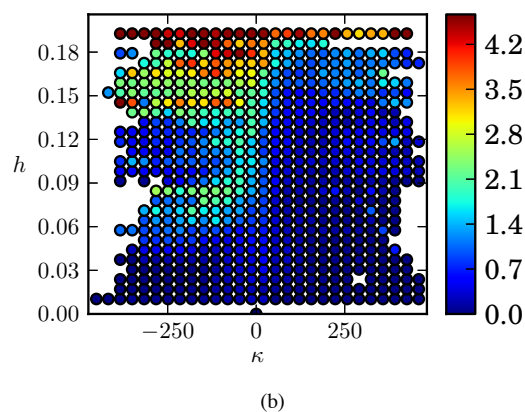
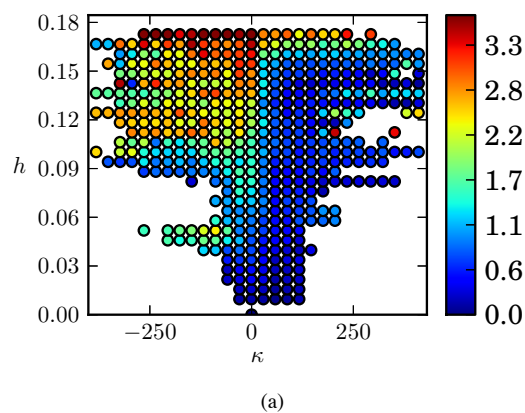


Figure 4: Map of  $\chi$  with respect to  $\kappa$  and  $h$ . Bivariate bins (with respect to  $\kappa$  and  $h$ ) are established. Points are binned and if a set of points exists within the bin the shear rate is averaged and that point is displayed on the map.

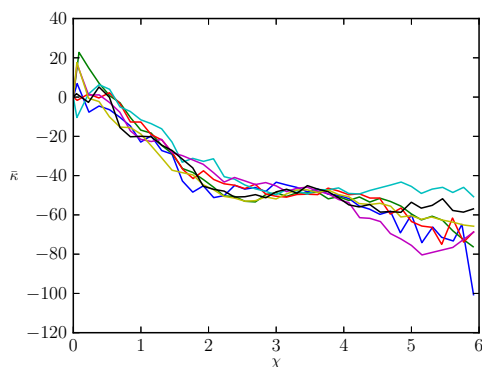


Figure 5: Plots of curvature versus shear rate on the thrombus surface. Each point on the surface is binned based on the shear rate. The curvature values within the bin are averaged. Each coloured curve represents one of the thrombi simulated in this study.

## Acknowledgements

This research was supported by a Victorian Life Sciences Computation Initiative (VLSCI) grant numbers VR0023 and VR0025 on its Peak Computing Facility at the University of Melbourne, an initiative of the Victorian Government, Australia. CJB thanks the Monash Engineering Faculty for the ERLA funding his study.

## References

- [1] Born, G. V. R. and Cross, M. J., The aggregation of blood platelets, *J. Physiol.*, **168**, 1963, 178–195.
- [2] Butler, C., Ryan, K. and Sheard, G., Haemodynamic forces on in vitro thrombi: a numerical analysis, *Med. Biol. Eng. Comput.*, **50**, 2012, 493–502.
- [3] Butler, C. J., Ryan, K. and Sheard, G. J., Shear rate gradients within an in vitro thrombotic environment, in *Proceedings of the Seventeenth Australasian Fluid Mechanics Conference*, editors G. D. Mallinson and J. E. Cater, The University of Auckland ISBN: 978-0-86869-129-9, The University of Auckland, Auckland, New Zealand, 2010, Paper 193, Paper 193.
- [4] Butler, C. J., Sheard, G. J. and Ryan, K., Modelling variations in shear rate around a geometrically similar thrombus in-vitro, in *Seventh International Conference on Computational Fluid Dynamics in the Minerals & Process Industries*, editors P. J. Witt and M. P. Schwarz, CSIRO Australia, Rydges Hotel, Melbourne, Australia, 2009.
- [5] Foundation, O., *OpenFOAM – The Open Source Computational Fluid Dynamics (CFD) Toolbox – User Guide*, 2.1.0 edition, 2011.
- [6] Goncalves, I., Nesbitt, W. S., Yuan, Y. and Jackson, S. P., Importance of temporal flow gradients and integrin  $\alpha\text{IIb}\beta_3$  mechanotransduction for shear activation of platelets, *J. Biol. Chem.*, **280**, 2005, 15430–15437.
- [7] Ku, D. N., Blood flow in arteries, *Annu. Rev. Fluid Mech.*, **29**, 1997, 399–434.
- [8] Kulkarni, S., Nesbitt, W. S., Dopheide, S. M., Hughan, S. C., Harper, I. S. and Jackson, S. P., Techniques to examine platelet adhesive interactions under flow, *Methods Mol. Biol.*, **272**, 2004, 165–186.
- [9] Nesbitt, W. S., Westein, E., Tovar-Lopez, F. J., Tolouei, E., Mitchell, A., Fu, J., Carberry, J., Fouras, A. and Jackson, S. P., A shear gradient-dependent platelet aggregation mechanism drives thrombus formation, *Nat. Med.*, **15**, 2009, 665–673.
- [10] Rodkiewicz, C. M., Sinha, P. and Kennedy, J. S., On the application of a constitutive equation for whole human blood, *J. Biomech. Eng.-T ASME*, **112**, 1990, 198–206.
- [11] Savage, B., Saldivar, E. and Ruggeri, Z. M., Initiation of platelet adhesion by arrest onto fibrinogen or translocation on von Willebrand factor, *Cell*, **84**, 1996, 289–297.
- [12] Silicon Graphics International Corp., OpenFOAM®– the open source computational fluid dynamics (CFD) toolbox, 2012, <http://www.openfoam.com>.
- [13] Tolouei, E., Butler, C. J., Fouras, A., Ryan, K., Sheard, G. J. and Carberry, J., Effect of Hemodynamic Forces on Platelet Aggregation Geometry, *Ann. Biomed. Eng.*, **39**, 2011, 1403–1413.